

AN ABSTRACT OF THE THESIS OF

Dara L. Easley for the degree of Honors Baccalaureate of Science in Physics presented on February 7, 2003. Title: Room Temperature Seebeck Measurements on $\text{CuSc}_{1-x}\text{Mg}_x\text{O}_{2+y}$ Transparent Conductive Thin Films.

Abstract approved:

Janet Tate

A series of seven magnesium-doped copper scandium oxide films were made by radio frequency sputtering, and intercalated at various oxygen pressures to create different oxygen concentrations in each film. The objectives of this study were to verify the p-type nature of these transparent conductive thin films, to determine the correlation between the Seebeck coefficients and the oxygen intercalation pressures, and to extract an estimate of the carrier concentration. Results of the room temperature Seebeck measurements show that the p-type nature of the carriers persists for all intercalation pressures. Small Seebeck coefficients characteristic of metals corresponded to high oxygen intercalation pressures, whereas larger coefficients characteristic of semiconductors corresponded to low intercalation pressures. One film exhibited intermediate values. Further analysis of the Seebeck coefficients using the Chaikin/Beni method gave reasonable qualitative values for the carrier concentrations of the films.

© Copyright by Dara L. Easley
February 07, 2003
All Rights Reserved

Room Temperature Seebeck Measurements on
 $\text{CuSc}_{1-x}\text{Mg}_x\text{O}_{2+y}$ Transparent Conductive Thin Films

by

Dara L. Easley

A PROJECT

submitted to

Oregon State University

University Honors College

in partial fulfillment of
the requirements for the
degree of

Honors Bachelors of Science in Physics (Honors Scholar)

Presented Feb. 07, 2003
Commencement June 2003

Honors Bachelor of Science in Physics project of Dara L. Easley presented on Feb. 07 , 2003

APPROVED:

Mentor, representing Physics

Committee Member, representing Physics

Committee Member, representing Physics

Chair, Department of Physics

Dean, University Honors College

I understand that my project will become part of the permanent collection of Oregon State University, University Honors College. My signature below authorizes release of my project to any reader upon request.

Dara L. Easley, Author

ACKNOWLEDGEMENT

I would like to thank Janet Tate, Bill Warren, and Allen Wasserman for all of their contributions and support. They read several versions of this thesis and offered many valuable suggestions. They also helped me gain a better theoretical understanding of carrier movement theory. This thesis is definitely a product of an exceptional team.

I would like to further thank Janet for her endless hours of help throughout the entire research and thesis process. She was patient with my numerous questions and always made time for me. Janet is an excellent research mentor, and she demonstrates quality leadership in an experimental research team. I am fortunate to have had the opportunity to work with her and to observe her as a dedicated professor and researcher.

Additionally, I would like to thank my parents, family and friends for both supporting me through this endeavor and being understanding about all of the time I had to commit. Your emotional support was invaluable.

TABLE OF CONTENTS

	<u>Page</u>
INTRODUCTION.....	1
Problem Definition	1
Statement of Purpose	2
Overview of this Paper.....	3
THEORY	4
Seebeck Theory	4
Thermocouple Theory.....	6
Thermocouples Used in This Experiment	9
DESCRIPTION OF EXPERIMENT	13
Materials.....	13
Seebeck Apparatus.....	15
DATA COLLECTION	19
LabVIEW Program.....	19
Procedure for Taking Room Temperature Seebeck Data	22
Raw Data Results.....	23
DATA ANALYSIS	25
Procedure for Analyzing Data.....	25
Results.....	26
Discussion of Results.....	28
Carrier Concentration	32

TABLE OF CONTENTS (Continued)

	<u>Page</u>
TRANSPORT THEORY RELATING TO SEEBECK EFFECT.....	34
Introduction	34
Drude theory of metals.....	34
Sommerfeld theory of metals	37
Semiclassical theory of metals	38
Chaikin and Beni model.....	42
Discussion of Seebeck Coefficient	45
CONCLUSION.....	47
APPENDICES	
APPENDIX A: Results	A1
SM16a.....	A1
SM16b	A6
SM16c.....	A11
SM16d	A16
SM17a.....	A19
SM17b	A24
SM18d	A29
APPENDIX B: Summary of Trials.....	B1
APPENDIX C: Summary of Results	C1
APPENDIX D: LabVIEW Documentation.....	D1
APPENDIX E: Derivation of Equation (57) from Equation (54)	E1

LIST OF FIGURES

<u>Figure</u>	<u>Page</u>
1. Thermoelectric Circuit.....	4
2. Seebeck Voltage.....	4
3. Material B With Thermal Gradient	5
4. Example of Differential Thermocouple.....	6
5. Single Thermocouple.....	7
6. Differential Thermocouple	8
7. Type K Differential Thermocouple.....	9
8. Sample Differential Thermocouple.....	9
9. Delafossite Structure	13
10. Samples and Corresponding Oxygen Intercalation Pressures	14
11. Main Component of the Seebeck Apparatus	15
12. Schematic of Experimental Setup	17
13. Picture of Front Panel Display of Program.....	20
14. Flowchart of LabVIEW Program.....	21
15. Portion of One Data Set.....	23
16. Plot of data for Sample SM16a	24
17. Samples and Corresponding Oxygen Intercalation Pressures	27
18. Seebeck Coefficient vs. Oxygen Intercalation Pressures	27
19. Conductivity Data for CuScO ₂ Films.....	30
20. Lattice Data for CuScO ₂ Films	31
21. Results for Carrier Concentration Using Chaikin / Beni Analysis	33

LIST OF APPENDICES

<u>Appendix</u>	<u>Page</u>
A. Results	A1
B. Summary of Trials.....	B1
C. Summary of Results.....	C1
D. LabVIEW Documentation	D1
E. Derivation of Equation (57) from Equation (54)	E1

INTRODUCTION

Problem Definition

Solid-state materials are often characterized by their carrier transport properties. In addition to transferring electric charge, these carriers also transport energy, generating both electric and thermal currents. Transport properties provide information about the sign of the carriers, scattering mechanisms, Fermi Level, effective mass and band structure, which are essential for determining a material's applications (Young et al. 462).

We examined a series of transparent conductive oxide (TCO) thin films of $\text{CuSc}_{1-x}\text{Mg}_x\text{O}_{2+y}$, intercalated with oxygen at various pressures to change the oxygen content and thus the number of carriers. CuScO_2 is one of many metal oxides with low carrier mobility due to highly localized carriers. Traditionally, observation of the Hall effect is a useful method for analyzing carrier types. The Hall effect describes the transverse voltage generated by carriers when a current is passed through the sample and a magnetic field is applied perpendicular to the sample. Since the Hall voltage is determined by mobility, TCO materials often generate Hall voltages that are too small to measure. Seebeck measurements based on carrier movement due to a thermal gradient offer an effective alternative to Hall measurements on low mobility films. Specifically, the Seebeck effect gives the sign of the charge carriers and additional information about the state of the carriers, which is important to the basic understanding of the material and its applications.

Many opportunities for TCO applications exist in the electronics industry. To date, TCO materials have been used in touch screens, transparent window defrosters, flat

screen TVs and photovoltaic cells (solar cells). These applications require transparent materials with high enough conductivities that they function effectively as metals. For this reason, n-type TCOs are most commonly used since their conductivities exceed those of p-type materials by at least two orders of magnitude. The electronics industry is also interested in developing screens which contain transparent circuitry directly embedded for use in microdisplays and other screen applications. Since these applications would require p-n junctions, the search for transparent circuitry has created a push in the solid-state community to develop transparent p-type conductors that could be paired with the commonly used n-type transparent conductors.

Statement of Purpose

This research project had a series of objectives. The primary purpose was to determine the Seebeck coefficients, and therefore the signs of the carriers, in a series of TCO films. The secondary goal was to identify the correlation between these Seebeck coefficients and the pressure at which each sample was intercalated with oxygen, providing insight into the electronic state of the materials. In order to collect the necessary data, my immediate goal was to design a LabVIEW program that would interface with an existing experimental set-up to read and acquire the desired data in the computer. Lastly, I reviewed existing literature discussing the theoretical nature of carrier movement and the implications of knowing the carrier type, i.e. the additional information that could be extracted from the Seebeck coefficient.

Overview of this Paper

I will begin by providing a discussion of the theory involved in this experiment, namely the Seebeck effect and basic thermocouple theory. The following chapter describes the experimental set-up which includes a discussion of the materials examined and a detailed explanation of the apparatus. The *Data Collection* chapter explains the LabVIEW program that was used for taking data and provides a detailed flow-chart representing the programming routine. This chapter also describes the procedure that was followed during data collection. Additionally, an example of the raw data collected by the LabVIEW program is included at the end of the chapter. The *Data Analysis* chapter explains the procedure followed for analyzing the data and includes a discussion of the results. The final section, *Transport Theory Relating to the Seebeck Effect*, is theoretical in nature and examines further implications of the results in relation to carrier movement, as discussed in existing literature. I will end with a brief conclusion summarizing this project.

Appendix A contains all data and plots from my room temperature Seebeck measurements. A summary of the results from each trial appears in Appendix B. Additionally, a complete summary of the results in the form of an average Seebeck coefficient for each film appears in Appendix C. The complete documentation of my LabVIEW program, including a block diagram of the program, appears in Appendix D. Appendix E contains the derivation of the Chaikin and Beni equation which relates the Seebeck coefficient to the carrier concentration.

Seebeck Theory

In 1821, Thomas Seebeck designed a thermoelectric theory that would later become the basis for all thermocouples (The Temperature Handbook Z-13). Seebeck determined that a thermoelectric circuit could be made by heating the junction of two dissimilar metals, shown in Figure 1.

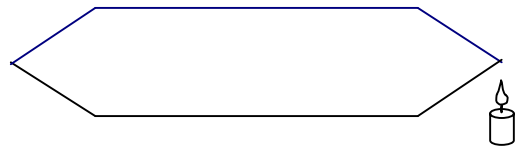


Figure 1 – Thermoelectric Circuit

An open thermoelectric circuit, shown in Figure 2, is commonly called a thermocouple. The voltage between the nodes of metals A and B can be measured experimentally, and is referred to as the Seebeck voltage.

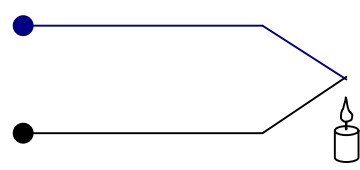


Figure 2 – Seebeck Voltage

The Seebeck voltage arises from the temperature gradient that develops across the circuit as the junction is heated. The Seebeck coefficient can be determined once the voltage and temperature gradient are known. For low mobility films, such as the p-type TCO thin

films examined in this experiment, the Seebeck coefficient is an alternative to the Hall coefficient for characterizing the material's transport properties. However, since different information can be extracted from each coefficient, Seebeck measurements do not replace Hall measurements.

In principle, a thermal gradient can develop across a single material as it is heated. Ideally, a Seebeck voltage exists across material B when a thermal gradient is present, as is shown in Figure 3. This voltage V satisfies Equation (1) where Q_B is the absolute thermopower, or Seebeck coefficient, of material B. The significance of the thermal gradient ΔT is discussed further in the *Thermocouple Theory* section.

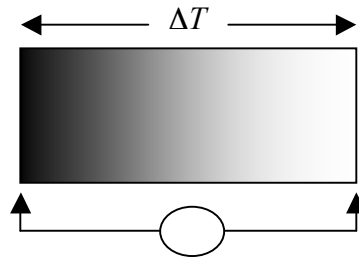


Figure 3 – Material B with Thermal Gradient

$$V = Q_B \Delta T \quad (1)$$

The voltage represented in Figure 3 is difficult to measure because wire leads of some material are necessary for connections with the voltmeter. The addition of such metal leads creates a new device shown in Figure 4, which is an example of a differential thermocouple.

$$V = \text{Seebeck voltage} = V_+ - V_-$$

Metal A Metal B

$$\alpha_{AB} = \text{Seebeck coefficient for Type AB thermocouple} = \alpha_A - \alpha_B$$

+ -
 T_{ref} V

$$\Delta T = \text{thermal gradient} = T - T_{ref}$$

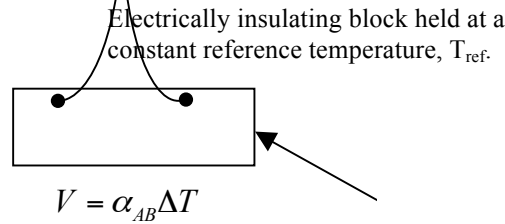


Figure 5 – Single Thermocouple

Metals A and B shown in Figure 5 have absolute thermopowers of α_A and α_B respectively. Additionally, thermocouple theory generally uses the convention that metal A is placed in the positive terminal of the voltmeter because the Seebeck coefficient of metal A is more positive than that of metal B. Evaluating V_+ and V_- produces Equations (2) and (3) respectively.

$$V_+ = \alpha_A (T - T_{ref}) \quad (2)$$

$$V_- = \alpha_B (T - T_{ref}) \quad (3)$$

Using Equations (2) and (3) and following the convention that $V = V_+ - V_-$, we can determine the Seebeck voltage, shown in Equation (4). Commonly, $(\alpha_A - \alpha_B)$ is replaced with α_{AB} , which produces Equation (5), a more familiar description of a single thermocouple.

$$V = (\alpha_A - \alpha_B)(T - T_{ref}) \quad (4)$$

$$V = \alpha_{AB}(T - T_{ref}) \quad (5)$$

Since α_{AB} is positive in standard commercial thermocouples by definition, the sign of the Seebeck voltage in the case of a single thermocouple is determined by the sign of

$+ V_1 - (T - T_{ref})$ and for $T_2 > T_{ref}$, the Seebeck voltage is positive.

The theory describing a differential thermocouple is derived from the addition of two single thermocouples, as shown in Figure 6. This step follows because the voltage between two ends depends only on the difference in the end temperature and is therefore path independent, as demonstrated in Equations (6) – (13).

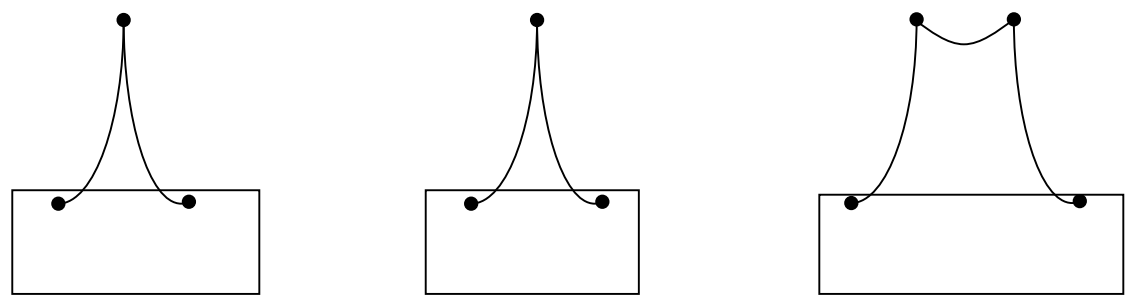


Figure 6 – Differential Thermocouple

Following the same conventions described for the case of the single thermocouple, the Seebeck voltage of the differential thermocouple can be determined. Solving for V_{1+} , V_{1-} , V_{2+} and V_{2-} as shown in Equations (6) – (9) allows for explicit determination of V.

$$V_{1+} = \alpha_A (T_1 - T_{ref}) \tag{6}$$

$$V_{1-} = \alpha_B (T_1 - T_{ref}) \tag{7}$$

$$V_{2+} = \alpha_B (T_2 - T_{ref}) \tag{8}$$

$$V_{2-} = \alpha_A (T_2 - T_{ref}) \tag{9}$$

Again, following the convention that $V = V_+ - V_-$, both V_1 and V_2 can be determined, shown in Equations (10) and (11).

$$V_1 = (\alpha_A - \alpha_B)(T_1 - T_{ref}) = \alpha_{AB}(T_1 - T_{ref}) \tag{10}$$

$$V_2 = (\alpha_B - \alpha_A)(T_2 - T_{ref}) = -\alpha_{AB}(T_2 - T_{ref}) \tag{11}$$

Summing Equations (10) and (11), the overall Seebeck voltage for the differential thermocouple can be determined, shown in Equations (12) – (14).

$$V = \alpha_{AB}T_1 - \alpha_{AB}T_{ref} - \alpha_{AB}T_2 + \alpha_{AB}T_{ref} \tag{12}$$

$$V = \alpha_{AB}(T_1 - T_2) \tag{13}$$

Note that Equation (13) describes the case where metal A is connected to both the positive and negative voltmeter terminals, with metal B in between.

Thermocouples Used in This Experiment

The Seebeck measurements taken in this experiment used both a known alumel-chromel-alumel differential thermocouple shown in Figure 7 and an unknown differential thermocouple composed of the TCO sample with copper leads shown in Figure 8. Note that the cold block with corresponding temperature T_{Cold} is connected to the positive input.

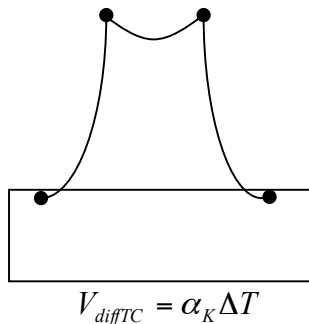


Figure 7 – Type K Diff. Thermocouple

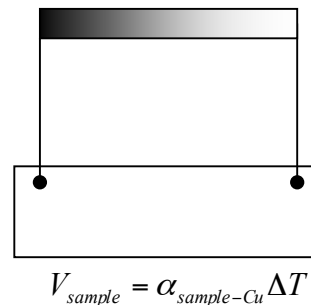


Figure 8 – Sample Diff. Thermocouple

A chromel-alumel thermocouple is commonly called a Type K thermocouple and the corresponding Seebeck coefficient, α_K , can be found in a reference text. The Temperature Handbook published by Omega Engineering, Inc. lists this value as

approximately $40 \mu V / K$ at room temperature (“Temperature” Z-18). The Seebeck coefficient of copper, α_{copper} , is small – typically a few $\mu V / K$. At room temperature, α_{copper} is approximately $2 \mu V / K$ (Seeger 94). Using the Seebeck coefficients for Type K, E and T thermocouples and taking $\alpha_{copper} \approx 2 \mu V / K$, the individual Seebeck coefficients of alumel and chromel can be approximated. This method yields Seebeck coefficients of $\alpha_{alumel} \approx -16 \mu V / K$ and $\alpha_{chromel} \approx 24 \mu V / K$.

A known thermocouple serves as a reference for comparison with an unknown thermocouple because both thermocouples measure the same thermal gradient. By measuring V_{diffTC} and referencing the value of α_K , we can determine the thermal gradient which is present. Once this value is determined, we can measure the voltage across the sample and calculate the Seebeck coefficient for the sample/copper device. This method for determining the Seebeck coefficient of the TCO film is described in further detail in the *Procedure for Analyzing Data* section of this paper.

The equations for the thermocouples in Figures 7 and 8 were determined following the same treatment used in Figure 6. For the case of the alumel-chromel-alumel differential thermocouple, in comparison to Figure 6, metal A is alumel, metal B is chromel, T_1 is T_{Cold} and T_2 is T_{Hot} . Thus, Equation (13) becomes Equation (14).

$$V_{diffTC} = (\alpha_{alumel} - \alpha_{chromel})(T_{Cold} - T_{Hot}) \quad (14)$$

Since the Seebeck coefficient of chromel is more positive than that of alumel, approximately $24 \mu V / K$ and $-16 \mu V / K$ respectively, the Seebeck coefficient for a type K thermocouple is $\alpha_K = \alpha_{chromel} - \alpha_{alumel}$. Following this convention, the Seebeck voltage for our differential Type K thermocouple can be simplified, as shown in Equations (15)

and (16).

$$V_{diffTC} = -\alpha_K(T_{Cold} - T_{Hot}) = \alpha_K(T_{Hot} - T_{Cold}) \quad (15)$$

$$V_{diffTC} = \alpha_K \Delta T \quad \text{for } \Delta T = T_{Hot} - T_{Cold} > 0 \quad (16)$$

The Seebeck voltage for the sample differential thermocouple shown in Figure 8 can be determined in a similar manner. Thus, for the sample differential thermocouple, Equation (14) becomes Equation (17).

$$V_{sample} = (\alpha_{copper} - \alpha_{sample})(T_{Cold} - T_{Hot}) \quad (17)$$

Further simplification results in Equation (18), which has the same thermal gradient as the Type K thermocouple described by Equation (16).

$$V_{sample} = (\alpha_{sample} - \alpha_{copper})\Delta T \quad (18)$$

$$V_{sample} = \alpha_{sample-Cu} \Delta T \quad (19)$$

Since ΔT is defined as $T_{Hot} - T_{Cold}$ and $T_{Hot} > T_{Cold}$, ΔT is always positive. Thus, following the aforementioned conventions, the sign of the Seebeck voltage will be determined by the Seebeck coefficient $\alpha_{sample-Cu} = \alpha_{sample} - \alpha_{copper}$. Since this thermocouple is not a standard commercial thermocouple, but rather one containing an unknown sample, we do not know if $\alpha_{sample-Cu}$ is positive or negative. If $\alpha_{sample} > \alpha_{copper}$, both $\alpha_{sample-Cu}$ and the measured Seebeck voltage will be positive. However, if $\alpha_{sample} < \alpha_{copper}$, both $\alpha_{sample-Cu}$ and the measured Seebeck coefficient will be negative.

The convention of having the cold block of temperature T_{cold} connected to the positive terminal of the voltmeter used in the experimental setup allows a positive voltage reading to correspond to a p-type sample if $\alpha_{sample} > \alpha_{copper}$. As the hot block is heated, the carriers in the material become energetic. Since the concentration of the excited

carriers near the hot block is greater than that near the cold block, carriers will diffuse toward the cold block. In the case of p-type conductivity, where holes are the carriers, this movement results in a higher hole concentration at the cold block and an absence of holes, or presence of electrons, at the hot block. This charge separation forms an electric field that opposes the carrier diffusion. By convention, the electric field points from positive to negative charge, so our convention of having the cold block connected to the positive voltmeter terminal causes the resulting voltage to be positive for $\alpha_{sample} > \alpha_{copper}$. Thus, following this convention, a positive Seebeck voltage corresponds to a film exhibiting p-type conductivity, with a Seebeck coefficient greater than that of copper.

DESCRIPTION OF EXPERIMENT

Materials

The material composition and structure of the series of TCO films I examined were selected by my research team, based on the findings of Kawazoe et al. in 1997. Knowing that in oxides, carriers tend to be strong localized, and that the valence band is strongly oxygen-like in character, Kawazoe et al. examined materials and structural configurations that would modify the energy band structure and reduce localization (Kawazoe et al. 940).

In an article discussing p-type electrical conduction in transparent thin films, Kawazoe et al. concluded that materials of the form CuMO_2 , where M is a trivalent cation, offered promising results in theory (Kawazoe et al. 940). Although pure CuMO_2 is insulating, carriers can be introduced by doping which will result in a conducting film. Kawazoe et al. also examined the crystal structure of the candidate oxides in search of a configuration that enhanced the covalency in the bonding between the copper and oxide ion (Kawazoe et al. 940). This condition led Kawazoe's group to select CuAlO_2 with the delafossite structure, shown in Figure 9.

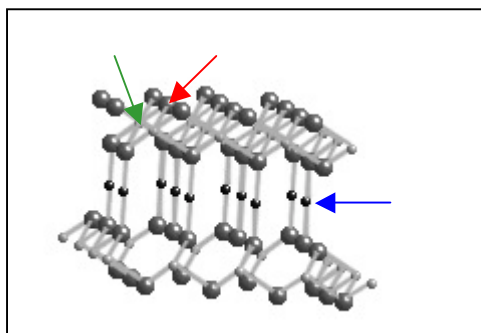


Figure 9 – Delafossite Structure



16d	16c	17a	17b	18d	16a	16b		14
0	2	3	50	120	15515	77573	(Torr)	

The research team that I worked with selected Sc as the M cation because its lattice structure responded well to the addition of oxygen atoms during intercalation. Specifically, the size of the Sc cation is large enough to allow oxygen to enter the structure. This addition of oxygen introduces holes into the valence band, which contributes to higher conductivities for the material.

In order to examine the correlation between a film's transport properties and its oxygen concentration, a series of $\text{CuSc}_{1-x}\text{Mg}_x\text{O}_{2+y}$ films was prepared by Andrew Draeseke. The CuScO_2 material was deposited onto a fused SiO_2 substrate by radio-frequency sputtering in argon gas, with further heat treatment. Intercalating oxygen into the films at a constant temperature of 400°C and at various O_2 pressures created the different oxygen concentrations. This increased the O_2 concentration of the $\text{CuSc}_{1-x}\text{Mg}_x\text{O}_{2+y}$ films to values between $y = 0.0$ and 0.5 , determined by x-ray measurements. The resulting films varied in color, ranging from transparent insulating films to darker conductive films. Profilometer measurements determined that the films ranged in thickness between 200 and 250 nm. Figure 10 displays each film with its corresponding film name and oxygen intercalation pressure.

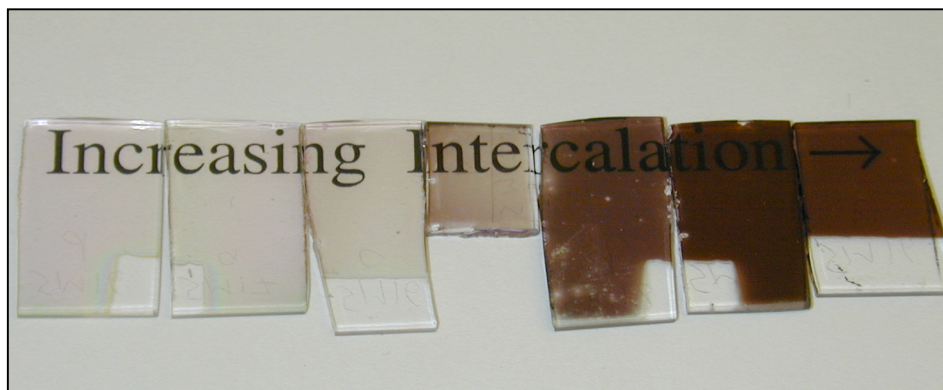


Figure 10 – Samples and Corresponding Oxygen Intercalation Pressures (Note: Samples 16c and 17a are interchanged in this photo, although labels and corresponding pressures remain correct.)

Sample **Seebeck Apparatus**

Cu Blocks

Teflon Sheet

Heat Sinks

The Seebeck apparatus was constructed by Till Ulbrich, based on a similar system described by Young (Young et al. 462). Much of the design is not applicable to the room temperature measurements that I took, but is necessary for temperature dependent measurements of the Seebeck coefficient. A schematic of the main component of the Seebeck apparatus is provided below.

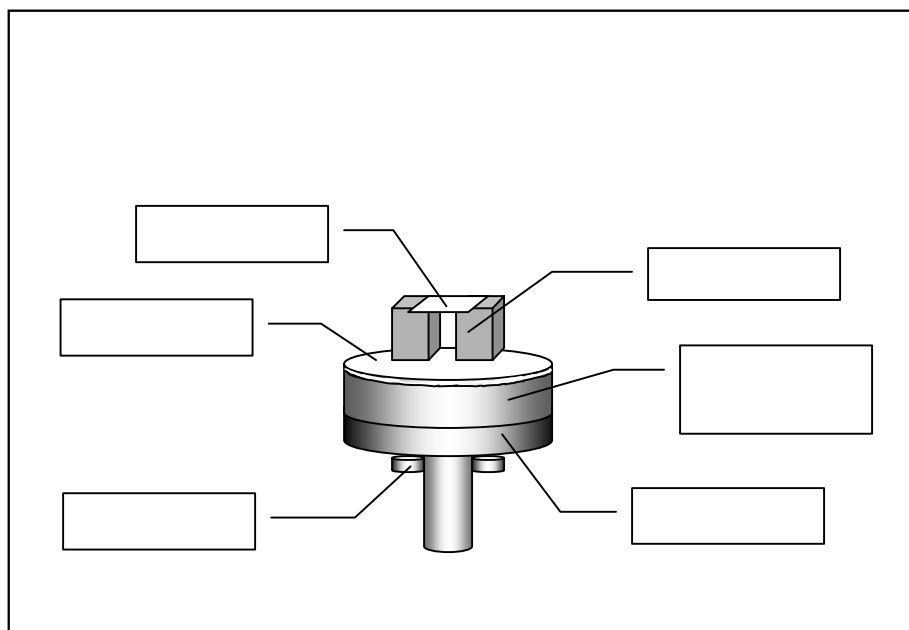


Figure 11 – Main Component of the Seebeck Apparatus

The experiment was assembled in a Janis cryostat connected to a closed cycle helium refrigerator to provide ambient temperatures from room temperature to 10K. The cryostat also provides protection from drafts, lighting, etc. when experiments are being conducted at room temperature. The sample mount consisted of two copper blocks separated by a thin Teflon sheet from a copper thermal reservoir. Ulbrich found that a Teflon sheet thickness of 0.7mm provided the necessary electrical insulation between the

copper blocks and the thermal reservoir. The chosen thickness was thin enough to maintain sufficient thermal contact for the blocks to be heated and cooled together in a reasonable time, yet thick enough so that the blocks could be heated individually when generating a thermal gradient (Ulbrich 6). The film being measured was mounted film-side down, with only a small strip of area in contact with each copper block. A narrow strip of electrically insulating material fitted with screws covered the two edges of the film in contact with the block. Tightening the screws put more pressure on the sample, allowing for better electrical connection between the blocks. Copper wire attached to both copper blocks measured the voltage across the sample, which was read by a Keithley 195A multimeter. This created a copper-sample-copper thermocouple, whose Seebeck voltage is described by Equation (19).

$$V_{sample} = \alpha_{sample-Cu} \Delta T \quad (19)$$

One copper block was designated as the “hot block” and the other as the “cold block.” The hot block was heated using a 25Ω resistor that had been epoxied into the block and connected to a voltage source. Stycast™ epoxy was used to maintain thermal contact between the resistor and the block, while providing electrical insulation. A differential alumel-chromel-alumel thermocouple (Type K) was epoxied into both blocks to measure the Seebeck voltage between the hot and cold block. The Seebeck voltage for the differential thermocouple, described by Equation (16), was measured on a Tektronix DM5120 multimeter.

$$V_{diffTC} = \alpha_K \Delta T \quad (16)$$

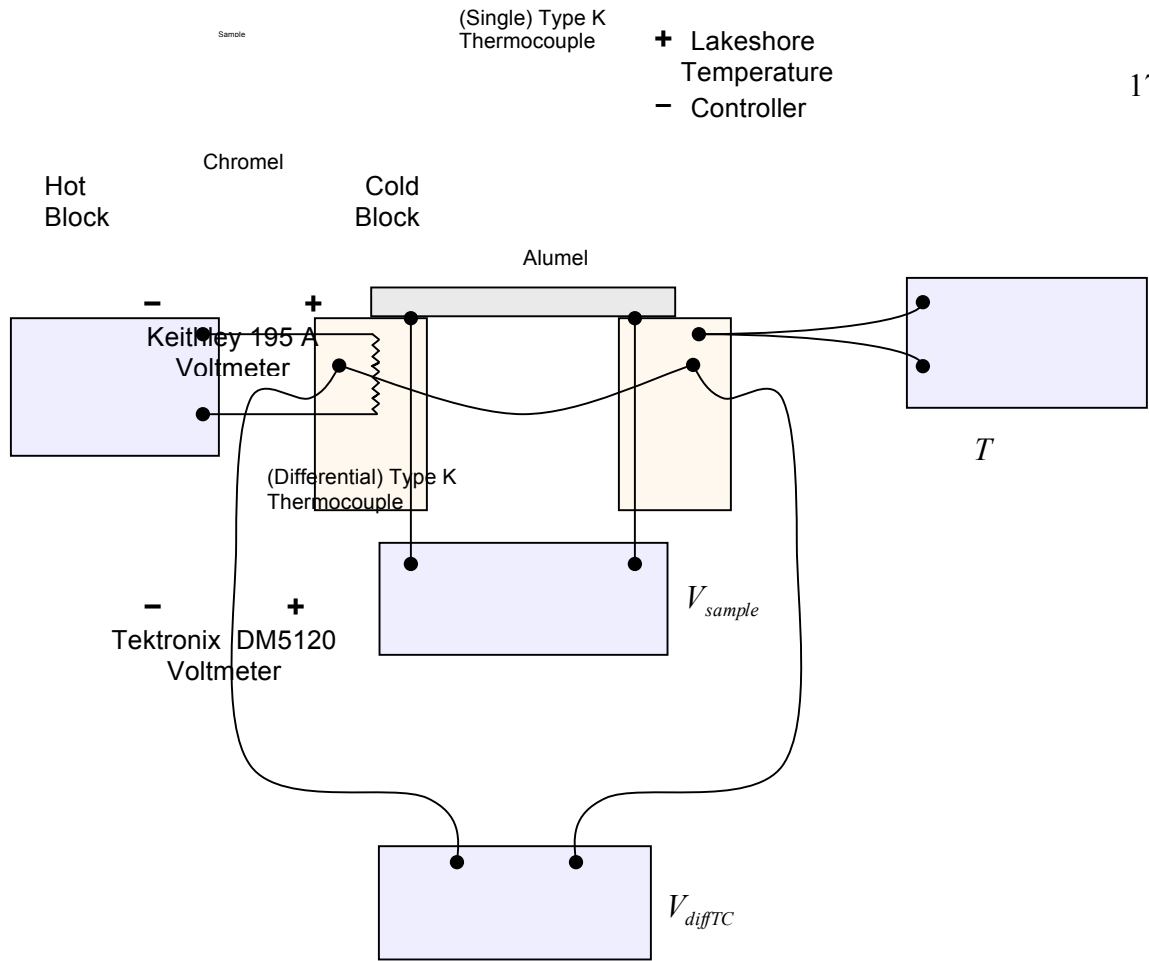
Figure 12 is a basic schematic showing how the meters were connected in the experimental setup.

Keithley 2400
Voltage
Source

+

-

Alumel



(Single) Type K
Thermocouple

+ Lakeshore
Temperature
Controller

Figure 12 – Schematic of Experimental Setup

Additional components of the apparatus are necessary for low-temperature measurements. A silicon diode was placed near the heat sinks, shown in Figure 11, to monitor the temperature of the cold head. Both the silicon diode and the heat sinks were held into place by Teflon tape, to ensure optimal thermal contact with the cold head. The ambient temperature inside the cryostat was determined using a single Type K thermocouple which was epoxied into the cold copper block. The thermocouple voltage was read by a Lakeshore temperature controller which converted the reading to a temperature. Again, the goal was to have all components of the apparatus at roughly the ambient temperature, with only a small temperature gradient induced between the copper blocks. To ensure that this was the case when taking temperature dependent

measurements, the ambient temperature reading could be continually monitored and compared with the temperature of the cold head.

All wires in the sample mount exited the cryostat by means of a multi-pin connector, which was wired to the multimeters. Each meter was assigned a GPIB address for interfacing with the computer. The LabVIEW data collection program used these addresses to initialize, read and source the meters.

A coaxial cable connected to the Keithley meter used for measuring the voltage across the sample was extremely sensitive to outside movement. Therefore, a low-noise cable was used to minimize the effect of external activity, such as people walking near the meters, which could potentially influence the measurements.

DATA COLLECTION

LabVIEW Program

The data for this experiment was acquired using a program created in LabVIEW, a National Instruments software package. I modified an existing LabVIEW program used for taking resistivity measurements with another apparatus. The program creates a “virtual instrument” that allows the user to view data on a control panel, just as he/she might if using an actual meter. LabVIEW can operate on many platforms; the measurements in this experiment were taken in LabVIEW 3.0, running on a Macintosh Quadra 800 with a general purpose interface bus (GPIB). I rewrote the program so that the computer would continually read data from the meters and perform a number of functions, which I will describe in further detail.

The control panel displays the ambient temperature inside the cryostat (T), the voltage across the differential thermocouple (V_{diffTC}) and the voltage across the sample (V_{sample}) as numerics. The control panel also displays plots of V_{diffTC} vs. time and V_{sample} vs. time, with user-adjustable axis values so that adjustments can be made during data collection. The voltage applied to the resistor in the hot block to generate a temperature gradient can also be manipulated from the front panel. The user can select an appropriate range of values for using the slide bar, or simply type the exact desired voltage into a blank field. A picture of the front panel display is provided in Figure 13.

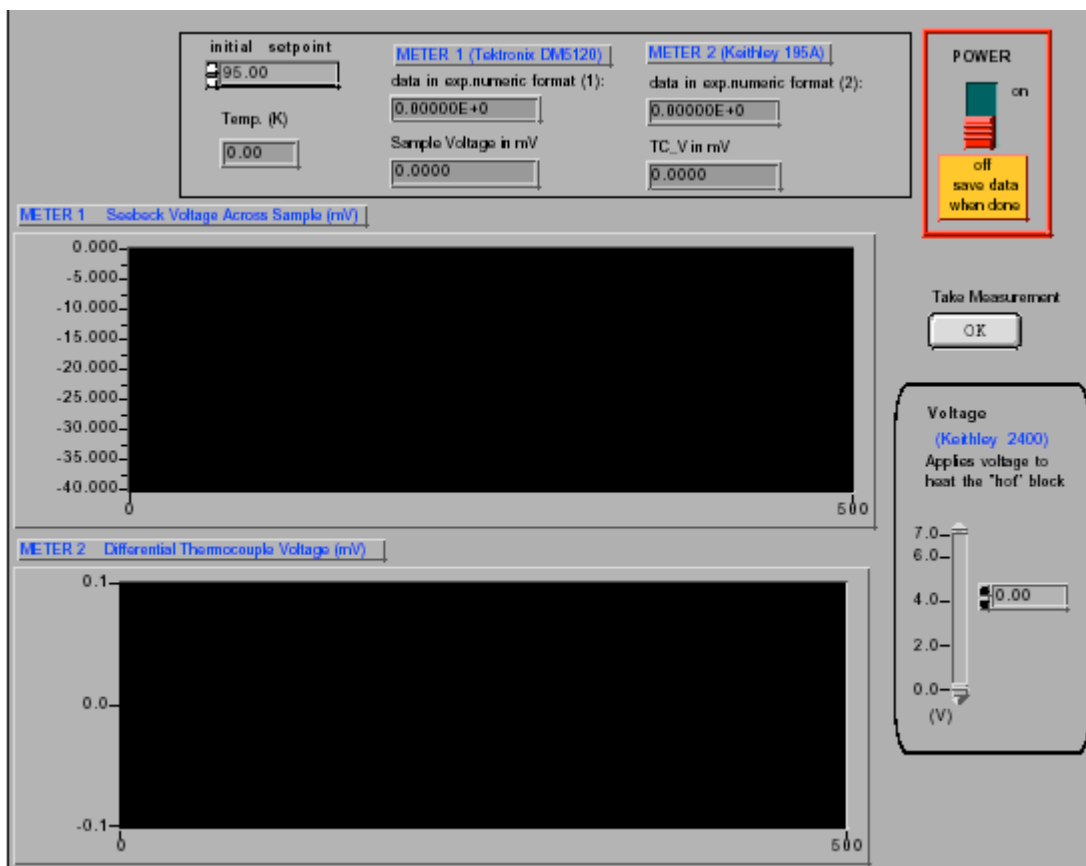


Figure 13 – Picture of Front Panel Display of Program

The program monitors voltage and temperature readings continuously. Upon reaching the conditions described in the *Procedure for Taking Room Temperature Data*, the user can click on the “Take Measurement” button which takes the last five data sets (T , V_{diffTC} , V_{sample}) and sends them to a storage array. When the user finishes data collection, he/she can close the program by clicking on the ON/OFF switch, upon which the user will immediately be prompted to type in a filename for saving the storage array. The saved data file can then be accessed in a data analysis/spreadsheet program for further manipulation. Figure 14 is a flowchart describing the process followed by the program. Additionally, a block diagram of the program shown in a visual object-oriented programming language is included in Appendix D.

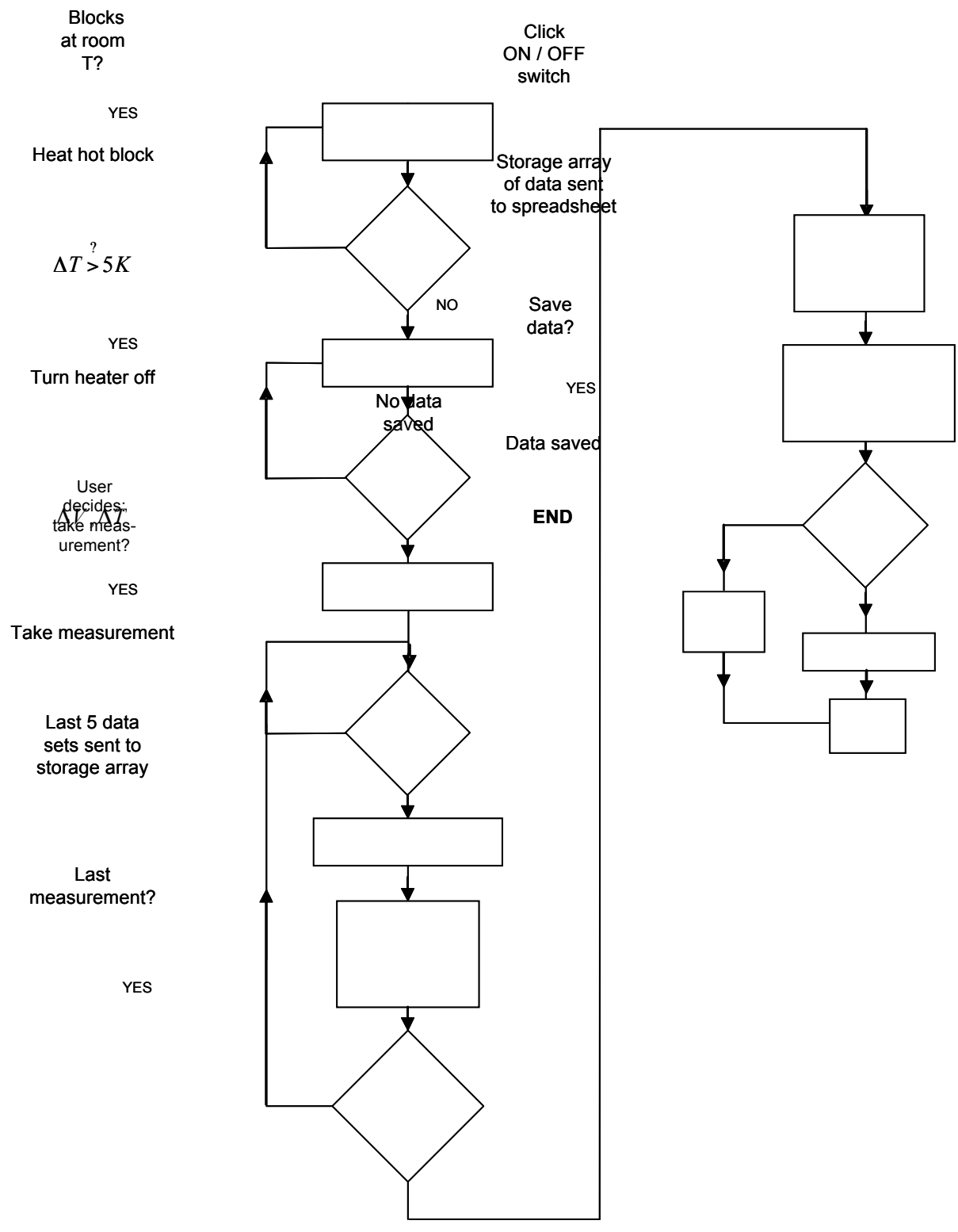


Figure 14 – Flowchart of LabVIEW Program

Procedure for Taking Room Temperature Seebeck Data

Prior to mounting the film sample, the surface of the copper blocks was sanded with fine sandpaper and swabbed with methanol to ensure a clean and grit-free surface. Next, the sample was securely mounted film-side down. I soldered indium contacts onto films SM16c and SM16d because they were too resistive to ensure good electrical contact with the copper blocks. I used indium from Lakeshore, model number IF-5. The soldering temperature for this indium is 252°C. Keeping the temperature just below the melting point of the solder made for an optimal bead.

These samples were carefully mounted film-side down with the indium contacts against the copper blocks. The remaining samples SM16a, SM16b, SM17a, SM17b and SM18d had no indium contacts. After the sample was mounted, the cryostat was closed and the LabVIEW program was started. Once the system had stabilized at a constant temperature and the meters had been zeroed, the Seebeck system was ready for data collection.

A voltage of five to seven volts was applied to the 25Ω resistor in the hot block, corresponding to current of 0.200 A to 0.280 A. The voltage was applied until the alumel-chromel-alumel differential thermocouple voltage reached approximately 200μV, which for a Type K thermocouple corresponds to roughly a 5 K temperature gradient between the hot and cold blocks, at room temperature. At this point, the source voltage was turned off causing the thermal gradient between the hot and cold blocks to decrease, and measurements of T , V_{diffTC} , V_{sample} were taken as the blocks cooled. The data was then saved and stored as a data file to later be analyzed in a spreadsheet application.

Raw Data Results

An example of one data set collected by the LabVIEW program is provided in Figure 15. The labels in Figure 15 are the following: **T** is the ambient temperature inside the cryostat measured in Kelvin, **V sample** is the voltage across the sample measured in Volts, and **TC_V** is the voltage across the differential thermocouple measured in Volts. Approximately five data sets were taken for each sample. Each data set was plotted in order to extract the Seebeck coefficient. Figure 16 is an example of such a plot corresponding to the data shown in Figure 15. The procedure for extracting the Seebeck coefficient from the plots is discussed in further detail in the *Data Analysis* section. All data and plots appear in Appendix A. A summary of results appears in Appendix C.

T	V sample (V)	TC_V
294.72	2.91E-04	2.10E-04
294.72	2.85E-04	2.07E-04
294.72	2.80E-04	2.05E-04
294.72	2.77E-04	2.01E-04
294.72	2.71E-04	1.97E-04
294.72	2.54E-04	1.86E-04
294.72	2.51E-04	1.81E-04
294.72	2.47E-04	1.79E-04
294.72	2.42E-04	1.77E-04
294.72	2.36E-04	1.74E-04
294.72	2.03E-04	1.46E-04
294.72	1.99E-04	1.46E-04
294.72	1.92E-04	1.43E-04
294.72	1.93E-04	1.42E-04
294.72	1.88E-04	1.38E-04
294.72	1.49E-04	1.09E-04
294.72	1.45E-04	1.06E-04
294.72	1.44E-04	1.04E-04
294.72	1.41E-04	1.04E-04
294.72	1.38E-04	1.02E-04

Figure 15 – Portion of One Data Set for Sample SM16a

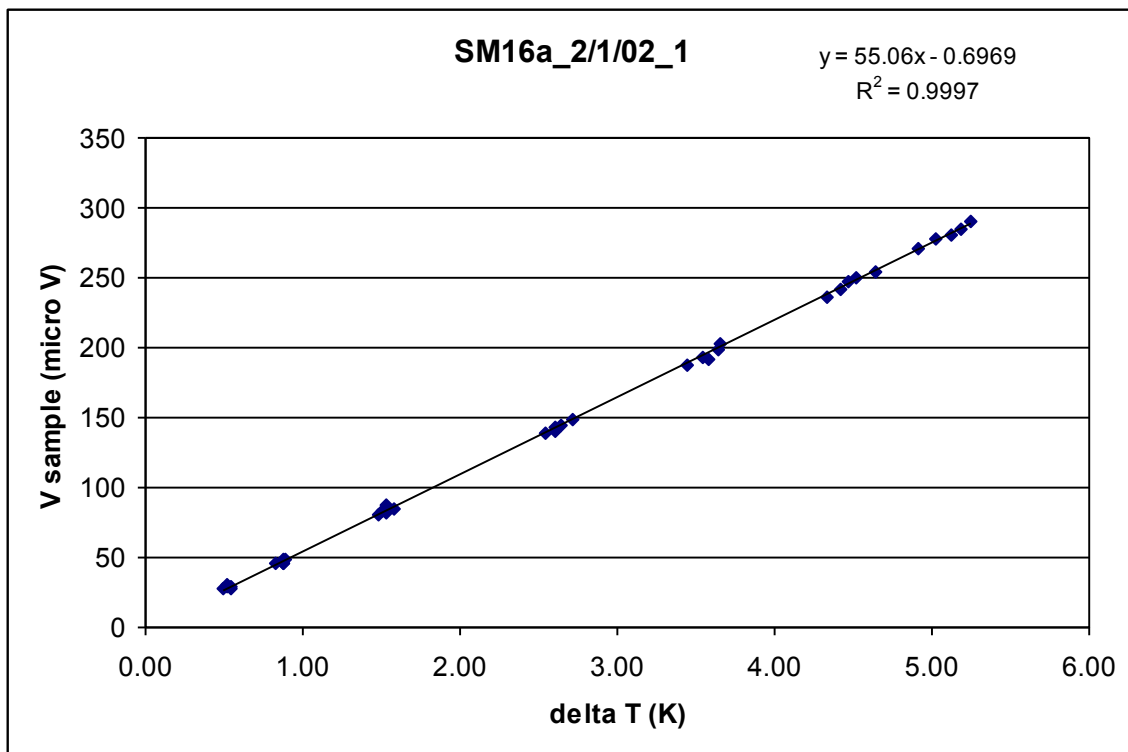


Figure 16 – Plot of data for Sample SM16a

DATA ANALYSIS

Procedure for Analyzing Data

The Seebeck voltage readings from the Type K differential thermocouple were used to determine ΔT , the temperature gradient between the hot and cold blocks, using the following equation:

$$V_{diffTC} = \alpha_K \Delta T \quad (16)$$

$$\alpha_K \approx 40 \mu V / K \quad (20)$$

Knowing ΔT , the Seebeck coefficient of the differential sample/copper thermocouple could be determined.

$$V_{sample} = \alpha_{sample-Cu} \Delta T \quad (19)$$

$$V_{sample} = \alpha_{sample-Cu} \left[\frac{V_{diffTC}}{\alpha_K} \right] \quad (21)$$

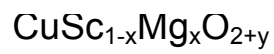
$$V_{sample} = \alpha_{sample-Cu} \left[\frac{V_{diffTC}}{40 \mu V / K} \right] \quad (22)$$

I found it easiest to plot V_{sample} vs. ΔT and then determine the slope, which is $\alpha_{sample-Cu}$, or $\alpha_{sample} - \alpha_{copper}$. I did not correct the Seebeck coefficients of the samples to account for the presence of copper for ease in comparison to existing data collected by other members on my research team. Thus, all Seebeck coefficients listed in the results on pages A-1 to A-36 include the Seebeck coefficient of copper.

Results

The results of this experiment are displayed in Appendix A. Approximately five data trials were taken for each film and a V_{sample} vs. ΔT plot appears below each corresponding data trial. The Seebeck coefficients were averaged to determine an overall average Seebeck coefficient for each film. The standard deviation between Seebeck coefficients for a given film was calculated for use with error bars in Figure 18. The averaging and standard deviation calculations appear in Appendix B. Additionally, a summary of results is included in Appendix C.

Figure 18 depicts the correlation between the average Seebeck coefficients and the oxygen intercalation pressures. It's important to note that the position of the data points in Figure 18 directly corresponds to the position of the samples in Figure 17.



16d	16c	17a	17b	18d	16a	16b	
0	2	3	50	120	15515	77573	(Torr)

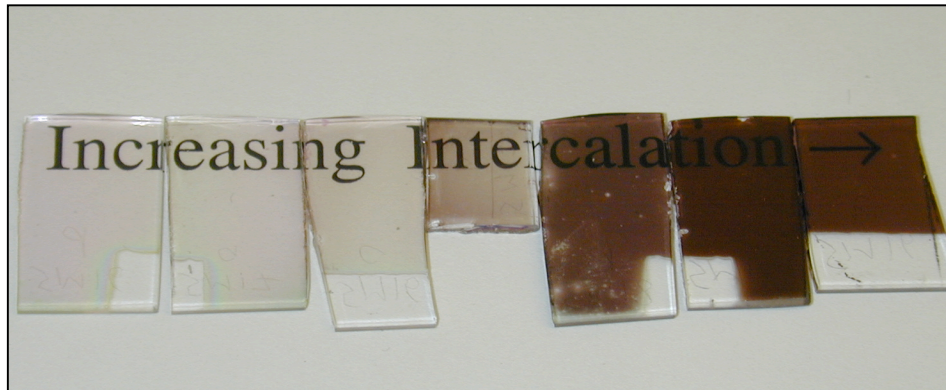


Figure 17 – Samples and Corresponding Oxygen Intercalation Pressures

Note: Samples 16c and 17a are interchanged in this photo, labels and corresponding pressures remain correct.

Seebeck Coeff vs. Intercalation Pressure

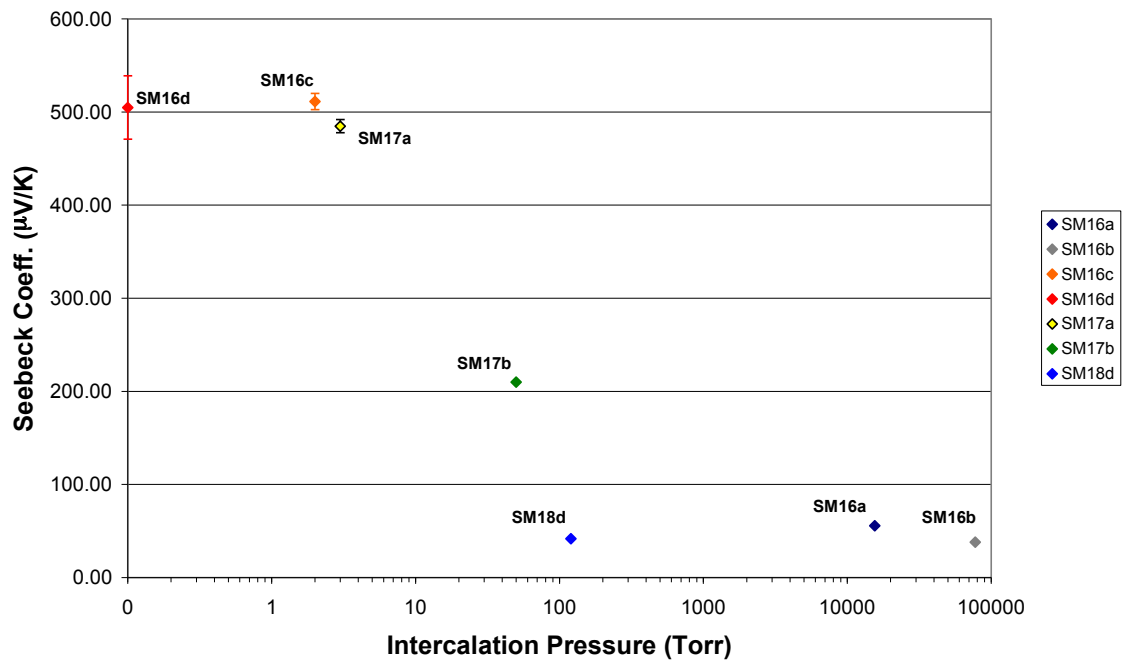


Figure 18 – Seebeck Coefficients vs. Oxygen Intercalation Pressures

Discussion of Results

The results of the Seebeck measurements provide us with a variety of information, when analyzed against the oxygen intercalation pressures. This information can be used along with results from optical measurements to characterize the properties of the films. The challenge of analyzing the Seebeck results is determining the extent of the information to be extracted from knowing the Seebeck coefficient. This is best examined by reviewing literature on transport theory, which I discuss in the *Transport Theory Relating to the Seebeck Effect* section. Note that the Seebeck measurements I took were at room temperature, therefore the Seebeck coefficients I refer to in this discussion are also at room temperature.

The Seebeck results show that the p-type nature of the carriers persists for all intercalation pressures. P-type nature corresponds to a positive Seebeck coefficient, meaning that holes are the electrical and thermal carriers in the film. It's important to note that a positive Seebeck coefficient does not mean that no n-type conductivity is present. Rather, a positive Seebeck coefficient demonstrates that p-type conductivity is the most dominant conductivity present in the film.

The results shown in Figure 18 also suggest that the seven $\text{CuSc}_{1-x}\text{Mg}_x\text{O}_{2+y}$ films examined in this experiment could be grouped into three categories based on the magnitude of the Seebeck coefficients at room temperature. The films SM18d, SM16a and SM16b correspond to Seebeck coefficients of approximately $50 \mu\text{V}/\text{K}$. Films SM16d, SM16c and SM17a correspond to Seebeck coefficients of approximately $500 \mu\text{V}/\text{K}$. Thus, these two groups of films have Seebeck coefficients which differ by approximately one order of magnitude. The third group contains only SM17b, which has

a Seebeck coefficient of approximately $210 \mu V / K$, an intermediate value in comparison to the other two groups of films.

Metals generally have small Seebeck coefficients, such as copper and silver whose Seebeck coefficients are less than $5 \mu V / K$. (Konstanz 2). This suggests that films SM18d, SM16a and SM16b are exhibiting more metallic characteristics in comparison to the other films. Materials such as silicon, which are intrinsically insulating but acquire semiconducting properties with the introduction of dopants, have Seebeck coefficients of several hundred $\mu V / K$. For example, the magnitude of room temperature Seebeck measurements of GaAs ranges between 200 and $400 \mu V / K$ (Tauc 248). Thus, the films SM16d, SM16c and SM17a appear to be exhibiting more semiconducting properties.

Since films SM16d, SM16c and SM17a were intercalated at lower oxygen pressures, we would like to correlate the semiconducting properties to low oxygen intercalation. Semiconductors characteristically have fewer mobile carriers in comparison to metals which typically have many highly mobile carriers. In order to confirm that the addition of oxygen via intercalation is in fact varying the number of mobile carriers present in the film, we can examine the conductivity data for the samples. This data was taken by other members of the research team and included in a paper, *P-type Conductivity in Transparent Oxides and Sulfide Fluorides*, submitted to the Journal of Solid State Chemistry in 2002 by the research team, H. Yanagi, S. Park, A. D. Draeseke, D. A. Keszler, and J. Tate. Figure 19 shows the conductivity data for the same films that I examined when taking Seebeck measurements. Note that SM16a and SM16b exhibit the highest conductivities and SM16d, SM16c and SM17a exhibit lower conductivities. As in Figure 18, SM17b also has an intermediate value in comparison to the other films,

approximate two orders of magnitude less than SM16a and SM16b, almost one order of magnitude greater than SM16c and SM17a, and nearly two orders of magnitude greater than SM16d.

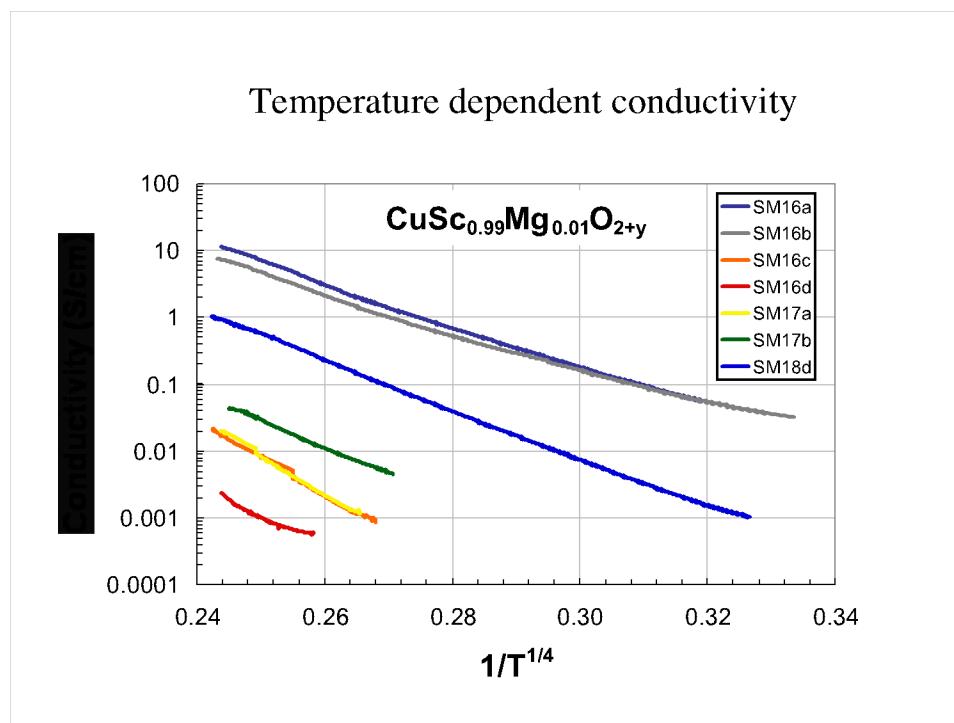


Figure 19 – Conductivity Data for CuScO_2 Films

Thus, we see that the films with lower Seebeck coefficients have higher conductivities, whereas the films with higher Seebeck coefficients have lower conductivities. This inverse correlation of Seebeck coefficients and conductivity confirms the hypothesis that films SM16b and SM16a are exhibiting more metallic properties, whereas films SM16d, SM16c and SM17a are exhibiting properties characteristic of semiconductors. Furthermore, these results suggest that the varying of oxygen intercalation pressures is in fact varying the number of carriers present in the films.

One way to further analyze the carrier concentration is by determining the lattice

parameter of each film. This is a worthwhile method, especially in the case of the delafossite structure, because the addition of carriers corresponds to an addition of oxygen molecules being forced into the lattice structure and thereby expanding it. In theory, as the oxygen molecules enter the structure, holes are created as the electrons rearrange. This addition of holes contributes to p-type conductivity. Thus, a large lattice parameter corresponds to a highly expanded crystal structure with many carriers present.

Figure 20, of the same source as the conductivity data, displays the lattice parameter data for the films determined by x-ray diffraction.

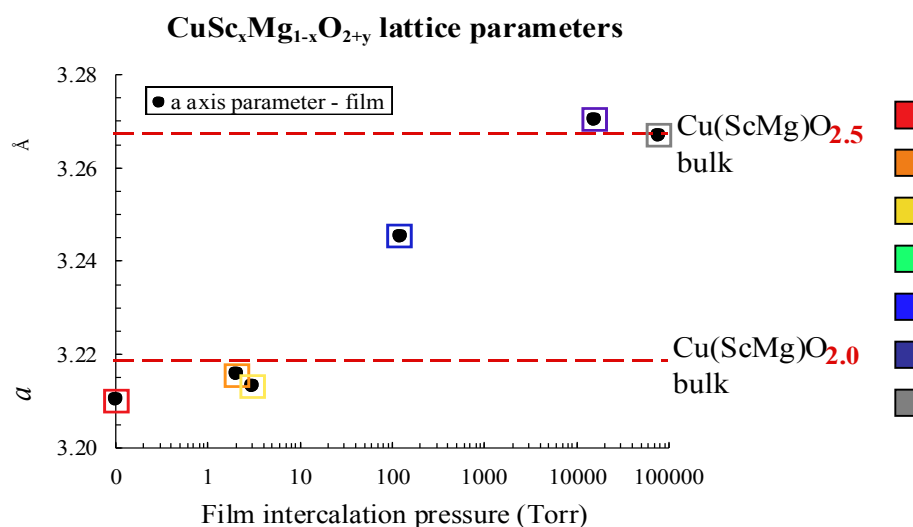


Figure 20 – Lattice Data for CuScO₂ Films (Note: Data unavailable for SM17b)

Note that SM16a and SM16b correspond to a larger lattice parameter of approximately 3.267 Å, whereas SM16d, SM16c and SM17a correspond to a smaller lattice parameter of 3.22 Å. This suggests that the oxygen intercalation did in fact introduce more carriers into films SM16a and SM16b, and fewer carriers into SM16d, SM16c and SM17a. Sample SM18d exhibited a lattice parameter of 3.245 Å, which is

intermediate of the aforementioned groups. Figure 20 does not display the lattice parameter of SM17b as it did not produce reliable x-ray diffraction data.

Additionally, it is important to note that the presumably insulating films are more transparent than the suggested metallic films, as shown in Figure 18. Since film SM17b has a Seebeck coefficient and conductivity intermediate to that of the other films, it appears as though SM17b is exhibiting properties intermediate to that of insulating and metallic materials, and likewise, intermediate properties of transparency and conductivity.

Carrier Concentration

According to the Chaikin and Beni theory discussed in the *Transport Theory Relating to the Seebeck Effect* section of this paper, it is possible to extract an estimate of the carrier concentration in the films from the Seebeck coefficient, assuming our system meets the criteria where this theory is applicable. Thus, assuming room temperature is high enough for the $\frac{S^{(2)}/S^{(1)}}{T}$ term to drop out of the Seebeck equation and assuming that hopping accounts for the carrier transport mechanism, we can make the following analysis.

Using the Chaikin / Beni model and solving for ρ , the carrier concentration, in terms of S , the Seebeck coefficient, results in the estimations for the carrier concentration shown in Figure 21. The Chaikin / Beni model was originally formulated for negative charge carriers. We have modified this model to create more general formulae in terms of the charge of the carriers, q .

Using Chaikin / Beni method

$$S = \frac{k_B}{q} \left(\log_e \cdot \frac{1-\rho}{\rho} \right)$$

FOR ELECTRONS**q** = charge of carrier 1.6E-19 C**k_B** = Boltzmann's Const. 1.38E-23 J/K

$$\rho = \frac{1}{1 + e^{\frac{k_B}{q} S}}$$

Where **ρ** is the ratio of particles to sites: $\rho = N/N_A$ **k_B/q** 86.17342 microV/K

Sample	Seebeck (microV/K)	Intercalation	
		Pressure (torr)	ρ_{hole}
SM16a	55.6	15515	0.344
SM16b	38.1	77573	0.391
SM16c	511.3	2	0.003
SM16d	504.8	0.1	0.003
SM17a	484.8	3	0.004
SM17b	209.9	50	0.080
SM18d	41.7	120	0.381

Figure 21 – Results for Carrier Concentration Using Chaikin / Beni Analysis

The results of the Chaikin and Beni analysis of the films show that the presumably more metallic films (SM16a, SM16b, SM18d) exhibit hole concentrations between 0.3 and 0.4, where as the presumably semiconducting films (SM16c, SM16d, SM17a) exhibit hole concentrations between 0.002 and 0.003. Additionally, as in the other analyses of Seebeck coefficient and conductivity, sample SM17b is again exhibiting a value intermediate to the other samples, namely 0.08 for the hole concentration.

TRANSPORT THEORY RELATING TO THE SEEBECK EFFECT

Introduction

A complete theoretical model describing the behavior of electrons or holes acting as thermal carriers in a semiconducting material extends beyond the scope of this undergraduate research project. Instead, I will examine the following theories describing generalized carrier movement and behavior in metals: the Drude Model and the Sommerfeld Model as discussed in Ashcroft and Mermin's Solid State Physics, and a semiclassical model as discussed in Ziman's Principles of the Theory of Solids. The semiclassical theory for metals comes closest to a complete description, but there is nonetheless a pedagogical value in examining the Sommerfeld and Drude models encountered in introductory physics.

Although the behavior of carriers in metals tends to be scattering, rather than hopping as in semiconductors, exploring these theories proves beneficial in determining the extent of the information to be gained from experimental measurements of the Seebeck coefficient.

Drude Theory of Metals

The Drude Model takes a classical approach to a situation which ultimately requires a quantum mechanical treatment due to the nature of the problem. Nonetheless, the Drude model yields results similar to those obtained experimentally and can therefore be used as a simplified model that does not consider quantum effects.

Drude formed his theory at the turn of the century, just three years after J.J.

Thomson discovered the electron in 1897. The Drude theory of metals considers electron interactions and movement to resemble that of the classical kinetics of rigid billiard balls. This classical Drude treatment is an independent electron model which neglects the details of electron-electron and electron-ion interactions, more formally referred to as the free electron approximation. Electrons are assumed to travel in a straight path until a collision of some unspecified origin occurs, which is considered to be an instantaneous event. This collision can be thought of as an average of all events that can take place. The rate at which electrons undergo such collisions, causing a change in velocity, is assumed to be $1/\tau$. The τ parameter is often referred to as the relaxation time or scattering time. This parameter is present in all the theories of metals and semiconductors that I examined, and is largely responsible for the uncertainty present in transport theory. The relaxation time cannot be directly measured or deduced experimentally. Rather, formulas in transport theory remain in terms of τ and experimentalists may substitute a speculative value if necessary. The last assumption present in Drude theory is that electrons reach thermal equilibrium with their surroundings via collisions. Thus, the velocity of the electron as it emerges from a collision is proportional to the temperature of the surroundings.

According to the previous assumptions, the electric current density \mathbf{J} present in the metal is given by Equation (23), where σ is the electrical conductivity and S is a coefficient.

$$\mathbf{J} = \sigma\mathbf{E} + S\nabla T \quad (23)$$

When no current is present, $\mathbf{J} = \mathbf{0}$, Equation (23) reduces to Equation (24), illustrating how an electric field can be generated by the presence of a temperature gradient.

$$\mathbf{E} = -Q\nabla T \quad (24)$$

The Q arises from combining the coefficients in Equation (23) and is often termed the “thermopower,” although it really is not a power at all. Rather, Q is the Seebeck coefficient of units $Volt/K$, represented by the character α earlier in this paper.

Using the equations given by the Drude model for the mean electronic velocity at a point x due to a temperature gradient v_Q , and the mean velocity due to an electric field v_E , we can determine what Q must be to have $v_Q + v_E = 0$, where v is the electron velocity.

$$v_Q = \frac{-\tau}{6} \frac{dv^2}{dT} \nabla T \quad (25)$$

$$v_E = \frac{-eE\tau}{m} \quad (26)$$

$$Q = \frac{-m}{6e} \frac{d}{dT} v^2 = \frac{-1}{3e} \frac{d}{dT} \left(\frac{1}{2} mv^2 \right) \quad (27)$$

In terms of heat capacity, Equation (27) reduces to Equation (28).

$$Q = \frac{-c_V}{3ne} \quad (28)$$

Drude evaluated Q using the classical interpretation of the specific heat, $c_V = \frac{3}{2} nk_B$,

which yields Equation (29).

$$Q = -\frac{k_B}{2e} \quad (29)$$

According to Ashcroft and Mermin, the result of Equation (29) causes Q to be larger than that observed in metals at room temperature. Note that Equation (29) depends only on Boltzmann’s constant and the value of the charge on an electron. Drude’s

classical assumption that the specific heat is given by $c_V = \frac{3}{2}nk_B$, as follows from the Maxwell-Boltzmann distribution, results in a lack of temperature dependence, as well as the absence of the relaxation time. Additionally, Drude's assumptions results in Q as always being negative, where as experimental results on various metals show that some metals may have a positive Seebeck coefficient. All of these inconsistencies suggest that the purely classical treatment for electrons eliminates some of the information necessary to provide an accurate description of carrier transport comparable that agrees with experimental findings.

Sommerfeld Theory of Metals

It wasn't until after the introduction of the Pauli Exclusion Principle that the transport theory inconsistencies began to be resolved. Sommerfeld applied the same theory to the free electron gas in metals by incorporating the Fermi-Dirac distribution into Drude's Theory of Metals in place of the Maxwell-Boltzmann distribution. The Fermi-Dirac statistics yield the specific heat shown in Equation (30), where ϵ_F is the Fermi energy.

$$c_V = \frac{\pi^2}{2} \left(\frac{k_B T}{\epsilon_F} \right) nk_B \quad (30)$$

Using this as the specific heat, c_V , in Drude's equation, Equation (28), results in a new formula describing the Seebeck coefficient, shown in Equation (31).

$$Q = -\frac{\pi^2}{6} \frac{k_B}{e} \left(\frac{k_B T}{\epsilon_F} \right) \quad (31)$$

Sommerfeld's description of the Seebeck coefficient resolves the overestimate made by Drude. Additionally, Equation (31) describes Q as having a temperature dependence which is not present in the Drude model. The sign problem present in Drude's theory is also resolved in Sommerfeld's interpretation. This is due to the quantum treatment of Fermi-Dirac statistics which allows for application to holes as well as electrons for carriers, whereas Drude's theory applied only to electrons. Thus, the carrier charge e could be positive or negative, depending on whether the material exhibits p-type or n-type conductivity.

Semiclassical Theory of Metals

Another treatment for transport properties was formulated after the advent of quantum mechanics. A number of theories explore this semiclassical theory, however I found the explanation in J. M. Ziman's Principles of the Theory of Solids to be most useful. This semiclassical argument centers on a transport equation, namely the Boltzmann equation. This equation incorporates a quantum perspective not present in the Drude or Sommerfeld models, by using a function that describes the average occupation of a given state k in a region around a point \mathbf{r} in space. Ziman uses $f_k(\mathbf{r})$ to denote the aforementioned function. This semiclassical approach to transport theory examines how $f_k(\mathbf{r})$ changes with time by analyzing what influences these changes.

One consideration is that $f_k(\mathbf{r})$ changes as carriers move in and out of the region near \mathbf{r} by diffusion. Another consideration is that external fields will change the k states of the carriers, thus altering the $f_k(\mathbf{r})$ distribution. The last consideration, scattering, is the most complex of the effects and is difficult to formulate theoretically. Focusing on a

state k , scattering describes the process of carriers in a state k changing to a state k' if vacancies are available in the k' distribution. Additionally, even if the vacancy exists, there is still a probability to consider of the k to k' event actually occurring. Processes can also cause transitions from occupied k' states to unoccupied k states. In the semiclassical treatment, $1/\tau$ is the difference between the two aforementioned rates.

Assuming the net change of $f_k(\mathbf{r})$ is zero for a specific k value at some point in space, as required by the Boltzmann equation, Equation (32) is formed.

$$\left. \frac{\partial f_k}{\partial t} \right]_{\text{scattering}} + \left. \frac{\partial f_k}{\partial t} \right]_{\text{external_fields}} + \left. \frac{\partial f_k}{\partial t} \right]_{\text{diffusion}} = 0 \quad (32)$$

The semiclassical theory of metals uses the above considerations to formulate the constraints of $f_k(\mathbf{r})$, which is taken to be the Fermi-Dirac distribution at equilibrium, denoted in Ziman's treatment as f_k^0 . A new function, $g_k(\mathbf{r})$ is introduced to describe how $f_k(\mathbf{r})$ departs from equilibrium, as described in Equation (33).

$$g_k = f_k - f_k^0 \quad (33)$$

Since f_k^0 is assumed to be defined temperature at a temperature T , it is likely that at temperature T , $f_k(\mathbf{r})$ may depart from f_k^0 , as shown in Equation (34). Thus, a temperature dependence is built into $g_k(\mathbf{r})$.

$$g_k(\mathbf{r}) = f_k(\mathbf{r}) - f_k^0\{\mathbf{T}(\mathbf{r})\} \quad (34)$$

By taking the total time derivative of $f_k(\mathbf{r})$, the Boltzmann equation can be formed. This process is described in Equations (35) through (40).

$$-\frac{\partial f_k}{\partial t} = -\left(\frac{\partial f_k}{\partial r} \cdot \frac{\partial r}{\partial t} \right) - \left(\frac{\partial f_k}{\partial k} \cdot \frac{\partial k}{\partial t} \right) \quad (35)$$

We can replace $\partial r/\partial t$ with v_K in Equation (35). Additionally, the $\partial k/\partial t$ term becomes eE/\hbar using the following reasoning shown in Equations (36) through (38).

$$\mathbf{F} = \frac{d}{dt}\mathbf{p} \quad (36)$$

$$e(\mathbf{E} + \mathbf{v} \times \mathbf{B}) = \hbar \frac{d\mathbf{k}}{dt} \quad (37)$$

$$\frac{d\mathbf{k}}{dt} = \frac{1}{\hbar}(e\mathbf{E} + e\mathbf{v} \times \mathbf{B}) \quad (38)$$

Thus, by replacing $\partial r/\partial t$ and $\partial k/\partial t$, Equation 36 becomes Equation (39).

$$-\frac{\partial f_K}{\partial t} = -\frac{\partial f_K}{\partial t} \cdot v_K - \frac{\partial f_K}{\partial t} \cdot \frac{1}{\hbar}(eE + e\mathbf{v} \times B) \quad (39)$$

Since the Seebeck effect occurs in the absence of a magnetic field, Equation (39) reduces to Equation (40).

$$-\frac{\partial f_K}{\partial t} = -\frac{\partial f_K}{\partial t} \cdot v_K - \frac{\partial f_K}{\partial t} \cdot \frac{eE}{\hbar} \quad (40)$$

Lastly, Ziman completes the equation by plugging in the partial derivatives of $f_K(\mathbf{r})$ in terms of f_K^0 , which I did not derive in this paper. This treatment can be viewed in detail in Ziman's text. The result is Boltzmann's equation in the absence of a magnetic field. Additionally, since $g_K(\mathbf{r})$ is incorporated into the equation, the temperature dependence and relaxation time are also being taken into account.

$$-v_K \cdot \frac{\partial f_K^0}{dT} \nabla T - \frac{e}{\hbar} E \left(\frac{\partial f_K^0}{dk} \right) = -\frac{\partial f_K^0}{dt} \Bigg]_{scatt.} + v_K \cdot \frac{\partial g_K}{\partial r} + \frac{e}{\hbar} E \left(\frac{\partial g_K}{\partial k} \right) \quad (41)$$

Ziman then manipulates Equation (41) until it can be placed in an integral to determine the current density. According to Ziman, he uses an integral similar to Equation (42).

$$\mathbf{J} = 2 \int e v_{\mathbf{k}} f_{\mathbf{k}} d\mathbf{k} \quad (42)$$

The result is shown in Equation (43), where the coefficients \mathbf{K}_n are tensors, which I won't describe here, as they are difficult to formulate.

$$\mathbf{J} = e^2 \mathbf{K}_0 \cdot \mathbf{E} + \frac{e}{T} \mathbf{K}_1 \cdot (-\nabla T) \quad (43)$$

Under the experimental conditions in which no current is allowed, the presence of an electric field results from the temperature gradient, as shown in Equation (44).

$$e^2 \mathbf{K}_0 \cdot \mathbf{E} = -\frac{e}{T} \mathbf{K}_1 \cdot (-\nabla T) \quad (44)$$

Solving Equation (44) for \mathbf{E} , and changing to scalar rather than tensor coefficients, results in Equation (45). Additionally, the leading terms form the Seebeck coefficient Q , as shown in Equation (46).

$$\mathbf{E} = \frac{1}{eT} \frac{K_1}{K_0} (\nabla T) \quad (45)$$

$$Q = \frac{1}{eT} \frac{K_1}{K_0} \quad (46)$$

Equation (46) does not clearly illustrate the temperature dependence of the Seebeck effect because it is unclear what the temperature dependence is for the K_n coefficients.

Chaikin and Beni Model

Although there is pedagogical value in examining the aforementioned theories of metals, it's important to remember that the samples examined in this experiment are not metals, but semiconductors. The carriers in metals are delocalized, and the resistance comes about because of scattering, involving carrier collisions with ions and defects. Scattering events occur relatively infrequently, in that carriers travel many lattice spaces before undergoing a collision. However, in many semiconducting materials, hopping replaces scattering as the carrier transport mechanism. Hopping is inherently quite different. Hopping can be thought of as a carrier becoming energetic enough to escape the potential energy well on the current atomic site and move to that of a nearby atomic site. Additionally, it is oftentimes energetically favorable for the carrier to tunnel to a nearby available atomic site, especially if the neighboring site exists at the same energy as the current site.

This combination of thermally activated motion and tunneling is often called Mott Variable Range Hopping and has a characteristic $1/T^{1/4}$ temperature dependence, as determined by N. F. Mott (Mott 32). Figure 19 suggests that the materials I examined exhibit this $1/T^{1/4}$ temperature dependence and thus suggests the carrier transport mechanism to be hopping.

P. M. Chaikin and G. Beni's paper "Thermopower in the Correlated Hopping Regime" appeared as the second of three consecutive papers discussing the theoretical nature of the Seebeck coefficient in various systems in the January 1976 issue of Physical Review B. (Note there is a small typographical error in the original paper, in that the minus sign appearing in front of the Seebeck equation should only be associated with the

first term of the sum.) Chaikin and Beni refer to the Seebeck coefficient as the “thermoelectric power” and take this to be given by Equation (47).

$$S = \frac{-S^{(2)}/S^{(1)} + \mu/e}{T} \quad (47)$$

The S transport coefficients are essentially the same as the K coefficients present in the semiclassical model discussed earlier. In the Chaikin and Beni model, $S^{(2)}$ is a heat term and $S^{(1)}$ is a current transport term. Additionally, e is taken to be the absolute value of the electron charge. Thus, Equation (47) is essentially the same as Equation (46) with the addition of the $\frac{\mu/e}{T}$ term, where μ is the chemical potential.

Chaikin and Beni’s argument is based upon a simplification of the Seebeck coefficient that occurs at high temperature. They argue that at high temperature, the $S^{(2)}/S^{(1)}$ term becomes temperature independent, causing the $\frac{S^{(2)}/S^{(1)}}{T}$ to be dominated by $1/T$. As T increases, this term will approach zero. However, the chemical potential term is strongly temperature dependent and is therefore not dominated by the $1/T$ term. Thus, as $T \rightarrow \infty$, Equation (47) becomes Equation (49).

$$S(T \rightarrow \infty) = -\frac{S^{(2)}/S^{(1)}}{T} + \frac{\mu}{eT} \quad (48)$$

$$S(T \rightarrow \infty) = \frac{\mu}{eT} \quad (49)$$

Equation (49) can be rewritten in terms of entropy according to the following derivation using the First Law of thermodynamics, where ζ is entropy, U is internal energy, V is volume. Additionally, entropy is taken to be that of Equation (53) in terms of the degeneracy, g .

$$Td\zeta = dU + pdV - \mu dN \quad (50)$$

$$d\zeta = \frac{1}{T} dU + \frac{p}{T} dV - \frac{\mu}{T} dN \quad (51)$$

$$-\left(\frac{\partial \zeta}{\partial N}\right)_{U,V} = \frac{\mu}{T} \quad (52)$$

$$\zeta = k_B \ln g \quad (53)$$

$$S(T \rightarrow \infty) = \frac{\mu}{eT} = -\frac{k_B}{e} \left(\frac{\partial \ln g}{\partial N} \right) \quad (54)$$

Chaikin and Beni use a simple statistical argument as shown in Equation (55) to determine the degeneracy, where $\rho = N/N_A$ denotes the ratio of particles to sites. Additionally, they use Stirling's approximation given in Equation (56) to arrive at equation (57). The full derivation appears in Appendix E.

$$g = \frac{N_A!}{N!(N_A - N)!} \quad (55)$$

$$\ln N! \approx N \ln N - N \quad (56)$$

$$S(T \rightarrow \infty) = -\frac{k_B}{e} \ln \left(\frac{1-\rho}{\rho} \right) \quad (57)$$

Equation (57) describes the Seebeck coefficient in terms of ρ , the electron concentration for high temperatures where the transport mechanism is considered to be hopping. Equation (57) can be rewritten to show the carrier concentration in terms of the Seebeck coefficient, as in Equation (58).

$$\rho = \frac{1}{1 + e^{\frac{-S}{k_B/e}}} \quad (58)$$

We can rewrite Equations (57) and (58) in a more general form using q to represent the

charge of the carriers, as shown in Equations (59) and (60), respectively.

$$S(T \rightarrow \infty) = \frac{k_B}{q} \ln\left(\frac{1-\rho}{\rho}\right) \quad (59)$$

$$\rho = \frac{1}{1 + e^{\frac{s}{k_B/q}}} \quad (60)$$

Discussion of Seebeck Coefficient

In comparison to Drude's and Sommerfeld's interpretation of Q , we see that the semiclassical method, as represented by Equation (46), offers a new insight, as long as one can interpret the K_n coefficients. Therefore, without a better understanding of the K_n coefficients, the complexity of the semiclassical method yields little to be extracted from the Seebeck coefficient besides the sign of the carriers. The information locked into the K_n coefficients is difficult, at best, to retrieve. As an undergraduate, I have not had the exposure to this level of applied mathematics in solid state theory to offer additional commentary on Equation (46).

Yet according to Chaikin and Beni, in materials where hopping is the carrier transport mechanism, at high temperature we need not consider the K_n coefficients, as they drop out, leaving a purely statistical argument. The materials examined in this experiment appear to meet the criteria of the Chaikin / Beni argument. Thus, only the following question remains: What is "high temperature?" Experimentally, this could be determined by examining temperature dependent Seebeck data. In theory, the temperature at which the Seebeck coefficient appears to become temperature independent corresponds to the situation required in the Chaikin / Beni methodology where the K_n coefficients are

temperature independent. Thus, the Chaikin / Beni method is an effective analysis of the Seebeck coefficients to determine carrier concentrations in this regime.

CONCLUSION

The Seebeck measurements I made on the seven $\text{CuSc}_{1-x}\text{Mg}_x\text{O}_{2+y}$ films verify that the films exhibit p-type conductivity. The magnitudes of the Seebeck coefficients suggest that samples SM16a, SM16b and SM18d have more metallic properties, whereas samples SM16c, SM16d and SM17a have coefficients characteristic of doped semiconductors. Sample SM17b exhibits an intermediate coefficient. Conductivity data taken by other members of my research team confirm these trends by showing that the metallic films exhibit significantly higher conductivities than the insulating films.

All experimental data supports the hypothesis that intercalating samples at varying oxygen pressures did in fact vary the number of carriers (holes) present in the films. The $1/T^{1/4}$ temperature dependence present in the log conductivity data strongly suggests hopping to be the transport mechanism present in the films, according to theory developed by N. F. Mott. Assuming that room temperature is high enough to meet the conditions required for the Chaikin / Beni theory, the Chaikin / Beni analysis becomes one method for estimating the hole concentration present in each of the films. Results of this analysis suggest the more metallic films to have hole concentrations greater than 0.35, whereas the insulating films have hole concentrations of approximately 0.003. Again, sample SM17b exhibits a concentration intermediate of the others, of approximately 0.08.

Future analysis of the Seebeck data using methodology similar to that of the Chaikin and Beni may provide additional information regarding the transport properties of these films.

APPENDIX A: Results

APPENDIX B: Summary of Trials

APPENDIX C: Summary of Results

APPENDIX D: LabVIEW Documentation

APPENDIX E: Derivation of Equation (57) from Equation (54)

BIBLIOGRAPHY

- Chaikin, P. M. and G. Beni. "Thermopower in the Correlated Hopping Regime." Physical Review B. 13 (1976): 647-651.
- Doumerc, Jean-Pierre. "Thermoelectric Power for Carriers in Localized States: A Generalization of Heikes and Chaikin-Beni Formulae." Journal of Solid State Chemistry. 110 (1994): 419-420.
- Emin, David. "Thermoelectric Power Due to Electronic Hopping Motion." Physical Review Letters. 35 (1975): 882-885.
- Gordillo, G., et al. "Characterization of SnO₂ thin films through thermoelectric power measurements." Thin Solid Films 342 (1999): 160-166.
- Isawa, Kazuyuki, et al. "Thermoelectric Power of Delafossite-derived Compounds." Physical Review B. 57 (1998): 7950-7954.
- Kasap, Safa. "Thermoelectric Effects in Metals: Thermocouples." e-Booklet. Mar. 2002 <<http://materials.usask.ca/server/kasap/Samples/Thermoelectric-Seebeck.pdf>>.
- Kawazoe, Hiroshi, et al. "Transparent p-Type Conducting Oxides: Design and Fabrication of p-n Heterojunctions." Materials Research Society Bulletin, Aug. 2000: 28-35.
- Kawazoe, Hiroshi, et al. "P-type electrical conduction in transparent thin films of CuAlO₂." Nature (1997): 939-942.
- Kubo, Ryogo, Mario Yokota and Sadao Nakajima. "Statistical-Mechanical Theory of Irreversible Processes." Journal of the Physical Society of Japan. 12 (1957): 1203-1211.
- Kudo, Atsushi, et al. "SrCu₂O₂: A p-type conductive oxide with wide band gap." Applied Physics Letters 73 (1998): 220-222.
- Kwak, J. F. and G. Beni. "Thermoelectric Power of a Hubbard Chain with Arbitrary Electron Density: Strong-Coupling Limit." Physical Review B. 13 (1976): 652-657.
- Kwak, J. F., G. Beni and P. M. Chaikin. "Thermoelectric Power in Hubbard-model Systems with Different Densities." Physical Review B. 13 (1976): 641-646.
- Marsh, D. B. and P. E. Parris. "Theory of the Seebeck Coefficient in LaCrO₃ and Related Perovskite Systems." Physical Review B. 54 (1996) 7720-7728.
- Mateeva, N., et al. "Correlation of Seebeck Coefficient and Electric Conductivity in Polyaniline and Polypyrrole." Journal of Applied Physics. 83 (1998): 3111-3117.

- Mott, N. F. Conduction in Non-crystalline Materials. Oxford: Clarendon Press, 1993: 32-35.
- Mott, N. F. "Conduction in Non-crystalline Materials." Philosophical Magazine. (1969): 835-852.
- Nell, J., et al. "Jonker-type Analysis of Small Polaron Conductors." Journal of Solid State Chemistry. 82 (1989): 247-254.
- Pálsson, Gunnar, and Gabriel Kotliar. "Thermoelectric Response Near the Density Driven Mott Transition." Physical Review Letters 80 (1998): 4775-4778.
- Rao, C. N. R., V. G. Bhide and N. F. Mott. "Hopping in $\text{La}_{1-x}\text{Sr}_x\text{CoO}_3$ and $\text{Nd}_{1-x}\text{Sr}_x\text{CoO}_3$." Philosophical Magazine. December (1975): 1277
- "The Seebeck Effect," Universität Konstanz website (Konstanz, Germany) , Nov. 2002. <<http://www.uni-konstanz.de/physik/Jaeckle/papers/thermopower/node1.html>>.
- Seeger, Karlheinz. Semiconductor Physics. New York: Springer-Verlag, 1973.
- Tauc, J. , ed. Amorphous and Liquid Semiconductors. London: Plenum Press, 1974: 248.
- The Temperature Handbook. Stamford: Omega Engineering, Inc., 1992.
- Ulbrich, Till. "Seebeck effect of transparent conductive oxides." Preprint of thesis, Universitaet Konstanz. July 7, 2001.
- Walstrom, P. L. "Spatial Dependence of Thermoelectric Voltages and Reversible Heats." American Journal of Physics. 56 (1988): 890-894.
- Yanagi, H., S. Park, A. D. Draeseke, D. A. Keszler, and J. Tate. "P-type Conductivity in Transparent Oxides and Sulfide Fluorides" submitted to Journal of Solid State Chemistry (2002).
- Ylilammi, Markku. "Properties of Silicon" Nov. 2002. <<http://www.geocities.com/SiliconValley/Bay/4104/silicon.html>>
- Young, D.L., et al. "Density-of-States Effective Mass and Scattering Parameter Measurements on Transparent Conducting Oxides Using Second-Order Transport Phenomena." Bulletin of Materials Science 25 (2002): 347-350.
- Young, D. L., T. J. Coutts, and V. I. Kaydanov. "Density-of-states effective mass and scattering parameter measurements by transport phenomena in thin films." Review of Scientific Instruments 71 (2000): 462-466.